J. Fluid Mech. (2003), *vol.* 491, *pp.* 239–258.
DOI: 10.1017/S002211200300541X Printed in the United Kingdom

Oscillatory thermocapillary convection in open cylindrical annuli. Part 1. Experiments under microgravity

By DIETRICH SCHWABE[1], ABDELFATTAH ZEBIB[2] AND BOK-CHEOL SIM[2]†

[1]I. Physikalisches Institut, Justus-Liebig-Universität, Heinrich-Buff-Ring 16, 35392 Giessen, Germany

[2]Department of Mechanical and Aerospace Engineering, Rutgers, The State University of New Jersey, Piscataway, NJ 08855-8058, USA

(Received 9 July 2001 and in revised form 23 April 2003)

We report results from microgravity experiments on thermocapillary convection in open annuli with outer radius $R_o = 40\,\text{mm}$ and inner radius $R_i = 20\,\text{mm}$ of various aspect ratios Ar. The measurements are from more than 230 equilibrated states in the Ar–Marangoni-number space. We found time-independent and oscillatory states and report some selected oscillation and Fourier spectra from thermocouple measurements. We measured the critical temperature difference ΔT^c for the onset of temperature oscillations in the range $1 \leqslant Ar \leqslant 8$. We report supercritical oscillation periods and attribute the oscillations in the larger Ar range to hydrothermal waves. This conclusion is supported by the values of the oscillation periods and of the critical Marangoni numbers in that Ar range. The hydrothermal waves exhibit an internal corotating multicellular pattern. For the smaller Ar and near the threshold we report m-fold temperature patterns on the free surface with m decreasing for decreasing Ar. At $4\Delta T^c$ these patterns become very irregular. Most of the findings are in accordance with the numerical results reported in Part 2 (Sim *et al.* (2003)). The experimental ΔT^c are higher and the experimental periods τ^c are smaller than the numerical values for Biot number $Bi = 0$. However, analysis of the experimental free-surface thermal boundary conditions shows that there was heat input to the free surface. Good agreement with numerical results for ΔT^c and τ^c is obtained with $Bi \neq 0$ (heat input).

1. Introduction

Fluid flow in the melt in a crucible from which a single crystal is grown by the Czochralski technique affects the crystal quality; for example time-dependent flow can result in inhomogeneous doping, reflecting this time-dependence by dopant striations. The main convective forces are (i) buoyancy, (ii) thermocapillarity and solutocapillarity, (iii) forced convection by crystal or crucible rotation, (iv) electromagnetic stirring, and (v) forced convection by crystal vibration. Forces (iii)–(v) are intentional whereas (i) and (ii) are inherent to the technique. The main aspects of the Czochralski technique are treated in Hurle & Cockayne (1994) and

† Present address: Department of Mechanical Engineering, Hanyang University, Ansan, Kyunggi-Do, 425-791, Korea.

thermocapillarity in crystal growth is dealt with in Schwabe (1988) and Kuhlmann (1999). Thermocapillarity is intimately coupled with buoyancy in the Czochralski system; there is heating from the outer wall and cooling in the centre and thus thermocapillarity is generated at the free upper annular melt surface. The horizontal radial temperature gradient gives rise to buoyancy as well. Because of this complexity we undertook an experiment under microgravity in a Czochralski-like configuration to study the flow structure of pure thermocapillary flow. The similarities between the Czochralski system and the present experiment can best be seen in figure 1 of Part 2 (Sim, Zebib & Schwabe 2003). The aspect ratio, the main geometry and part of the thermal boundary conditions are similar. Differences are found in the inner cooled wall, in the menisci at the outer and the inner walls, and in the thermal boundary conditions at the free surface which are strongly non-adiabatic for high-temperature melts.

A few attempts to study experimentally thermocapillary flow in an annular configuration under normal gravity and under microgravity have already been made. The first experimental work in shallow annular gaps to verify the theory by Smith & Davis (1983) was done by Schwabe (1984) and Schwabe *et al.* (1992); hydrothermal waves and surface waves were observed. Several experimental results on thermocapillary instabilities in open cylindrical containers are available. Thermocapillary instabilities in cylindrical vessels heated by a central cylinder with an aspect ratio near that of a Czochralski system have been reported by Kamotani, Lee & Ostrach (1992) and Favre, Blumenfed & Daviaud (1997). Some of this work is summarized in Busse, Pfister & Schwabe (1998). This Earth-bound work was limited to liquid heights $H \leqslant 3$ mm to reduce the influence of gravity. Because this cannot be avoided entirely and will be significant for $H > 3$ mm we planned our experiment under microgravity with larger H, the results of which are reported in this paper.

The recent microgravity experiment by Kamotani, Ostrach & Masud (2000) was similar to ours but used smaller and comparatively deeper containers and a higher-Prandtl-number fluid. In their experiments $Ar = (R_o - R_i)/H < 1$ whereas ours were in the range $Ar \geqslant 1$. From Smith & Davis (1983), Schwabe *et al.* (1992) and Riley & Neitzel (1998) it is known that the dimensional wavelength of the hydrothermal waves λ is $2.6H$. This means that only very few wavetrains in the azimuthal or radial directions can exist in an experiment with small R_i/H; the system will be 'frustrated', resulting possibly in a higher critical Marangoni number Ma^c. The strategy for our microgravity experiment was to ensure (at least in some experiments with small H) that the expected wavelength λ would be much smaller than $2\pi R_i$ and smaller than $(R_o - R_i)$; this would allow unhindered wave propagation in all directions and would make possible direct comparison with the existing theory for infinitely extended layers by Smith & Davis (1983). Deviations can be expected due to the radial symmetry of our experiment. We then proceed to experiments with higher H which is on the one hand the parameter region with strong influence of gravity on Earth and therefore normally not accessible, and on the other hand relevant to Czochralski crystal growth. The Czochralski growth situation is not comparable to extended layers and it is most likely that, due to the constraint $Ar \sim 1$ in this technique, thermocapillary structures other than hydrothermal waves will develop.

In contrast with Kamotani *et al.* (2000) who used a silicone oil with Prandtl number $Pr = 27$ in their experiment, we used the silicone oil with the lowest viscosity (0.65 cSt, $Pr = 6.8$) and are thus in the parameter region of important oxide melts and fluoride melts. The use of the highly volatile 0.65 cSt silicone oil posed an experimental problem, but this was overcome as discussed in detail below.

2. Experimental

The experiment MAGIA (Marangoni Grown Instabilities in an Annulus) was conducted on board on the Russian satellite FOTON-12 in September 1999. MAGIA was operated for 4 days under microgravity. The operation was mainly automatic. The free surface of the annular gap was observed with a normal CCD camera under diffuse illumination. The temperature at the free liquid surface was imaged by an IR camera. Temperatures were measured with fine thermocouples at five different locations in the fluid of the annulus.

We present the experimental results in dimensional form but in discussions and in comparison with Part 2, we use the following non-dimensional numbers:

Prandtl number $Pr = \nu/\alpha$,

Reynolds number $Re = \gamma \dfrac{\Delta T H}{\nu \mu}$,

Marangoni number $Ma = Pr\ Re = \gamma \dfrac{\Delta T H}{\alpha \mu}$,

Rayleigh number $Ra = \dfrac{g_0 \beta D^3 \Delta T}{\alpha \nu}$,

dynamic Bond number $Bo_{dyn} = Ra/Ma = \dfrac{g \beta \rho D^3}{\gamma H}$,

aspect ratio $Ar = (R_o - R_i)/H$,

where ν, α, μ, γ, β, ρ, g_0 are kinematic viscosity, thermal diffusivity, dynamic viscosity, negative temperature derivative of surface tension, volume expansion coefficient, density and normal Earth gravity. R_o and R_i are the outer and inner radii of the annular gap, H is the liquid height in the gap and ΔT is the temperature difference applied between the outer and inner walls. The residual gravity is g and D is the appropriate dimension in the direction of the residual gravity vector.

2.1. *The annular gap experiment MAGIA*

A sketch of the experiment MAGIA is given in figure 1. The vertical cross-section through the rotationally symmetric experiment chamber shows the annular gap with $R_o = 40\,\text{mm}$ and $R_i = 20\,\text{mm}$. The gap length $L = R_o - R_i = 20\,\text{mm}$ is fixed. The differentially heated (cooled) sidewalls are made of aluminium. The thermally insulating bottom of the gap was adjustable to liquid heights H, $2.5\,\text{mm} \leqslant H \leqslant 20\,\text{mm}$, and the injection (or retraction) of liquid was synchronized with the H-changes to ensure a 'flat-filled' gap (plane free surface and virtually no meniscus at the rim of the gap). An extra adjustment of the filling level by telesupport was possible and was carried out. The rims of the gap were sharp and their upper surface was painted with FC 725 from 3M-Company to avoid wetting by the oil and consequent capillary outflow under microgravity. A ZnS window allows the optical observation of the free surface of the gap from above and of its temperature distribution with an IR camera. The main experimental difficulty was the high vapour pressure of the 0.65 cSt silicone oil, comparable to that of pure ethanol. Without countermeasures all the liquid would have evaporated in typically 1–4 h and 'liquid bridges' of condensed oil could give rise to capillary outflow. We therefore heated all outer walls including the ZnS window to a temperature T_W of 30 °C, well above the temperature of the cooled inner cylinder, T_i. Thus all condensation of evaporated oil occurred at the top of

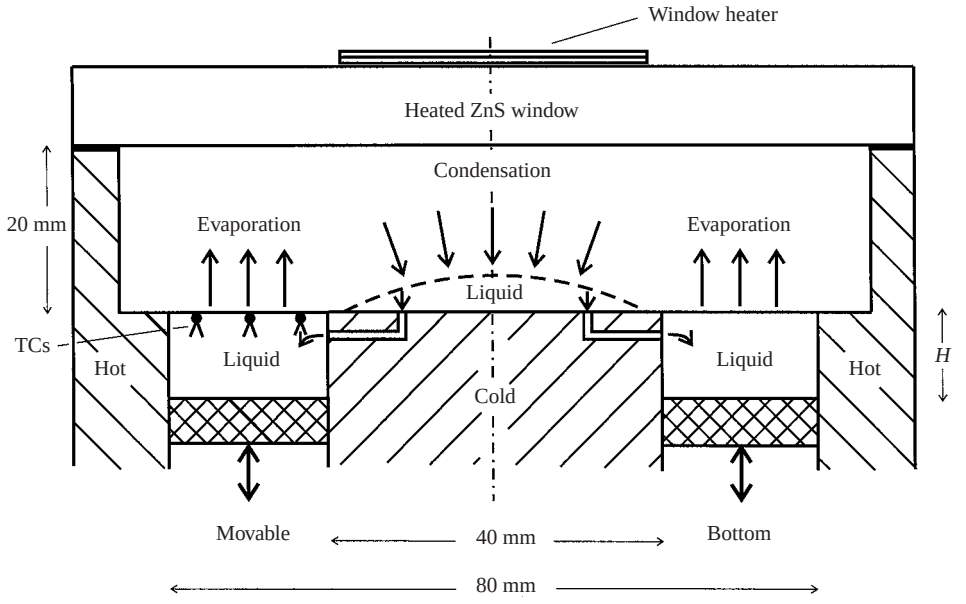

FIGURE 1. Sketch of the experiment MAGIA. The aspect ratio $Ar = (R_o - R_i)/H$ of the annular gap can be changed between 8 and 1 by adjusting H with a movable bottom. The free surface of the liquid was maintained flat by appropriate injection/retraction of liquid. Evaporated liquid condenses on the cold central cylinder and flows back into the gap through four channels due to capillary pressure.

Kinematic viscosity ν	6.5×10^{-7} m^2 s^{-1}
Thermal diffusivity α	9.5×10^{-8} m^2 s^{-1}
Prandtl number Pr	6.8
Surface tension σ	15.9×10^{-3} N m^{-1}
Temp. dependence of surface tension $\partial\sigma/\partial T$	-6.4×10^{-5} N m^{-1} K
Density ρ	760 kg m^{-3}
Temperature dependence of ρ	1.34×10^{-3} K^{-1}
Vapour pressure at 20 °C	2.6×10^{3} N m^{-2}

TABLE 1. Physical properties of the silicone oil $Si(CH_3)_3$–O–$Si(CH_3)_3$ at 25 °C.

the cold inner cylinder. There the condensed oil could accumulate a spherical section and flow back into the gap through four capillaries with wicks. The wicks were found to be mandatory for the filling of the capillaries from tests during parabolic flights. For the wick we used platinum wire 0.3 mm in diameter, touching the top of the cold cylinder. Due to surface tension there is a positive pressure in the spherical 'hat' and a slightly negative pressure in the gap due to its negative surface curvature when slightly underfilled. Thus the system is 'self-replenishing' and worked for days.

The relevant physical properties of the 0.65 cSt silicone oil are given in table 1. The mean temperature was held constant at $(T_o + T_i)/2 = 25\,^{\circ}$C.

2.2. *Accuracies, limitations and the microgravity environment*

The mechanical accuracies (proportions, parallelism of the bottom to the upper rim) of MAGIA were of the order of 0.01 mm. The underfilling was 1 cm^3, corresponding to a depression in microgravity of only 0.05 mm in the middle of the gap at $(R_o + R_i)/2$.

H (mm)	$Bo_{dyn} = \dfrac{g\beta\rho 27(R_o - R_i)^3}{\gamma H}$	$Bo^*_{dyn} = \dfrac{g\beta\rho 27(R_o - R_i)^4}{\gamma H^2}$
2.5	0.14	1.09
10	0.034	0.069
20	0.017	0.017

TABLE 2. Dynamic Bond numbers for three different values of H.

The temperature constancy of both sides T_o and T_i was such that the important temperature difference parameter $\Delta T = T_o - T_i$ was constant within ± 0.07 K after thermal equilibrium was reached. The ΔT values given as integers in the text and most figures (except figure 9 'critical $\Delta T = -\Delta T^{c}$') are the values calculated from the set point temperatures. The measured ΔT from sensors integrated into the sidewalls of the annulus are smaller by $\delta\Delta T$. For $H = 2.5$ mm and $\Delta T = 2$ K $\delta\Delta T$ is 0.15 K, increasing linearly to $\delta\Delta T = 0.3$ K for $\Delta T = 40$ K. For $H = 20.0$ mm and $\Delta T = 2$ K, $\delta\Delta T = 0.25$ K and for $\Delta T = 40$ K, $\delta\Delta T = 0.45$ K. Regular temperature oscillations due to oscillatory flow with an amplitude of 0.15 K were easily detected with the 0.25 mm diameter thermocouples in the liquid. The noise level of the amplified thermocouple signals was ± 0.05 K. The IR-camera had a temperature resolution of 0.1 K.

The accuracy of the microgravity level and the direction of the residual gravity during the flight are not known but a recent analysis showed that there were variable gravity disturbances of the order of $10^{-5}g_0$ during the flight of FOTON-12 (Sheftsova, Melnikov & Legros 2002). By far the largest gravity component occurred in the radial direction of MAGIA. The variation of this gravity component during flight inferred from the IR-pictures is documented in Schwabe & Benz (2002). For the worst case, estimates of the dynamic Bond number Bo_{dyn}, relating the influence of residual gravity $g = 10^{-5}g_0$ in the radial direction and the influence of thermocapillary forces, are given in table 2 for three different liquid heights. The dimension D in the Rayleigh number was taken as $3(R_i - R_o)$ to account for the geometry of the annular gap. A physically more relevant estimate of the thermocapillary effect can be made and is based on a different definition of the Marangoni number $M^* = \gamma\Delta T H^2/[(R_o - R_i)\alpha\mu]$ as in Smith & Davis 1983. The values of $Bo^*_{dyn} = Ra/M^*$ are given in table 2 as well.

The IR-camera detected non-rotationally symmetric temperature distributions on the free surface during many measurements (see one example in figure 12*d*) which can be explained by a radial gravity component.

2.3. *Measurement procedure*

The measurements under microgravity proceeded as follows: a liquid layer depth H was installed and then different temperature differences ΔT were realized for approximately 15 min each. These periods are called steps. During at least the last 6 min of each step the fluid system was in equilibrium; thermal equilibrium was typically reached 10 min before the end of the step. We took measurements of 230 different steps distributed in the parameter range $1\text{ K} \leqslant \Delta T \leqslant 40\text{ K}$ and $2.5\text{ mm} \leqslant H \leqslant 20.0\text{ mm}$. Temperature measurements with five thermocouples in the liquid, placed 1 mm below the free surface, were taken with a sampling frequency of 20 Hz during the last 6 min of each step. The thermocouple tips were located in different positions at ($r = 24$ mm, $\alpha = 0°$), ($r = 30$ mm, $\alpha = 0°$), ($r = 34$ mm, $\alpha = 0°$), ($r = 30$ mm, $\alpha = -17°$), ($r = 30$ mm, $\alpha = +5°$) to resolve by correlation analysis the wavy character of the

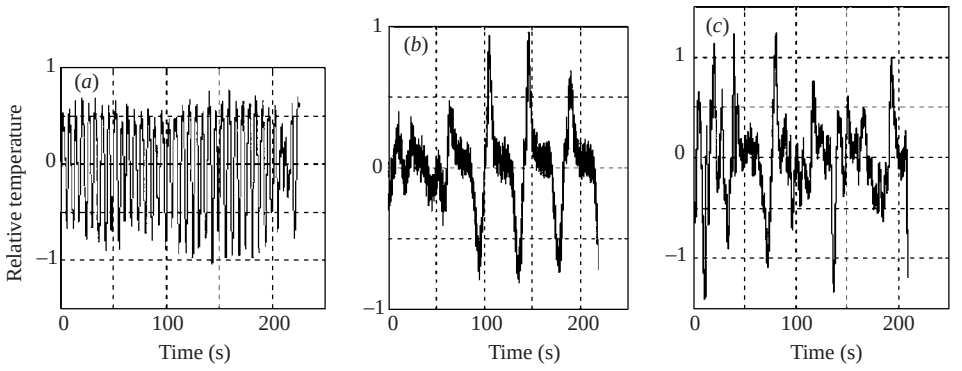

FIGURE 2. Temperature oscillations near the threshold. (*a*) $H = 2.5$ mm, $\Delta T = 4$ K, (*b*) $H = 6$ mm, $\Delta T = 2$ K, (*c*) $H = 20$ mm, $\Delta T = 4$ K. The typical noise level of the oscillation signal is ± 0.1 of the arbitrary temperature scale. The absolute maximum peak–peak amplitude is approximately 0.5 K in (*a*), 0.7 K in (*b*) and 0.8 K in (*c*).

oscillations. The azimuthal position $\alpha = 0^\circ$ corresponds to $\theta = \pi$ in Part 2. The IR-pictures were taken with 15 Hz during the final 5 s of each step.

3. Experimental results and discussion

We expect to observe oscillatory flow states corresponding to the hydrothermal waves in the flat annular gaps (small H or large Ar and $R_o \approx R_i$) because the return flow solution of Smith & Davis (1983) applies in this case. For smaller Ar different oscillatory states may occur. Thermocouple data are best suited in this experiment to characterize the temporal structure of the flow states and to determine the transition from time-independent to oscillatory flow. They are presented first. Then the structure of supercritical flow states as detected by the IR-camera from temperature distributions at the free surface is discussed. Finally we present and discuss some deviations from 'ideal' boundary conditions for a quantitatively more satisfying comparison of the experimental results and the numerical simulations in Part 2.

3.1. *Characterization of flow states by thermocouple measurements*

Among the 230 flow states (measurement steps) realized in the H–ΔT range, seven were time-independent because the applied temperature difference ΔT was only 1 K and thus below ΔT^c. For all other steps with $\Delta T \geqslant 2$ K the flow was oscillatory in the whole H range (except one measurement with $H = 2.5$ mm and $\Delta T = 2$ K).

Figure 2(*a–c*) shows three examples of the temperature–time signal near the threshold for the liquid heights $H = 2.5$ mm and $\Delta T = 4$ K, $H = 6.0$ mm and $\Delta T = 2$ K, $H = 20.0$ mm and $\Delta T = 4$ K. In these examples, the oscillations are well above the noise level which is in a much higher frequency band, best seen in figure 2(*b*). In figure 2(*b*) the oscillations have a period τ of approximately 40 s at the end of the measurement time with a peak–peak amplitude of approximately 1.5, whereas the noise has a peak–peak amplitude of 0.2 on the relative temperature scale. Microgravity disturbances in this frequency band can be excluded as the cause of such oscillations. The oscillations are regular only for the smaller H and small ΔT (figure 2*a*) and one can expect to extract a well-defined period τ or frequency f and Fourier amplitude from such a signal. The temperature–time trace in figure 2(*c*) with $H = 20$ mm and $\Delta T = 4$ K (aspect ratio $Ar = 1$) is taken at roughly two times the critical Reynolds number

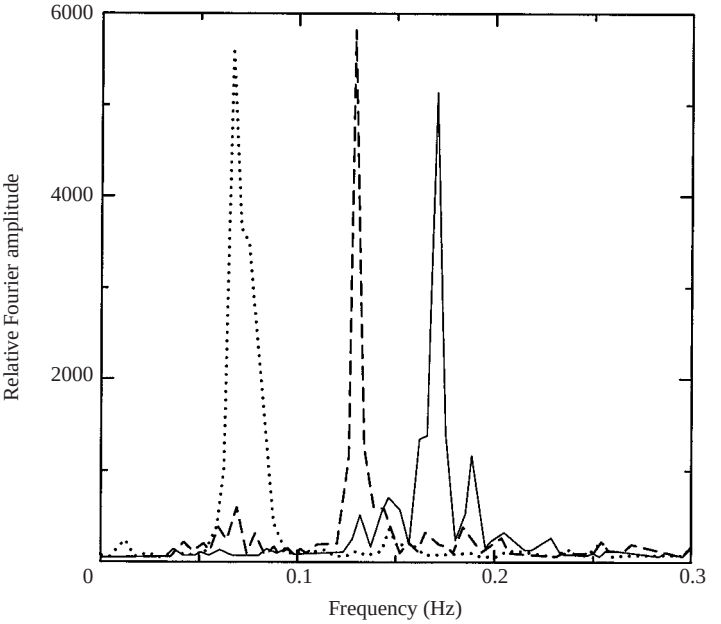

FIGURE 3. Fourier spectra of the thermocouple located at $r = 34$ mm, $\alpha = 0$ for $H = 3.0$ mm and $\Delta T = 2$ K (·····), $\Delta T = 5$ K (-----), and $\Delta T = 8$ K (—). The corresponding Fourier peaks of the main frequency have amplitudes of 18.2, 970, and 5100, respectively.

Re_c and is considerably more irregular than the equivalent case in the numerical simulation (Part 2, figure 3). This is typical for larger H and ΔT. But the irregularities of the temperature signal in figure 2(*c*) are not due to external disturbances.

The decrease in the frequency f with increasing H is also seen in figure 2. Here figure 2(*b*) is a special example of extremely low f for $H = 6.0$ mm, most probably due to $\Delta T = 2$ K being extremely near to the threshold ΔT^c. Figure 3 shows the Fourier analysis of the signals from the thermocouple placed at $r = 34$ mm and $\alpha = 0$ for $H = 3.0$ mm and the three temperature differences $\Delta T = 2$ K, 5 K and 8 K. The main oscillation frequency is well defined and increases with ΔT from 0.071 Hz to 0.171 Hz. The Fourier amplitude increases from 18.2 to 970 up to 5100. With increasing ΔT the spectra become more complex. Regular oscillations are found only for $H \leqslant 6.0$ mm. For $H > 6.0$ mm the temperature signals are more irregular, even near the threshold (figure 5). Figure 4 shows the Fourier spectra of the three thermocouples at the same azimuthal position $\alpha = 0°$ but different radial positions for the experiment with $H = 4$ mm and $\Delta T = 2$ K. We note that the Fourier amplitude A decreases from the inner cold wall ($r = 24$ mm, $A = 480$) towards the middle of the gap ($r = 30$ mm, $A = 230$) and to the outer hot wall ($r = 34$ mm, $A = 110$). This is an indication that the wave is travelling towards the hot wall as is the case for hydrothermal waves (Smith & Davis 1983); because we are near the threshold the wave might be excited only near the cold side. The same is observed in the simulations (Part 2, figures 7, 8, 9, 11, 12, 14). The more irregular oscillation spectra at higher supercritical Reynolds numbers are found in the smaller Ar range rather than in the larger range, both experimentally and numerically. In the range of larger Ar one can argue that the return flow solution of Smith & Davis (1983) no longer applies and a flow structure different from hydrothermal waves is established. For $Ar = 1$ the structure of the steady flow observed in the gap (Part 2, figure 17*a*) is very different from the simple return flow

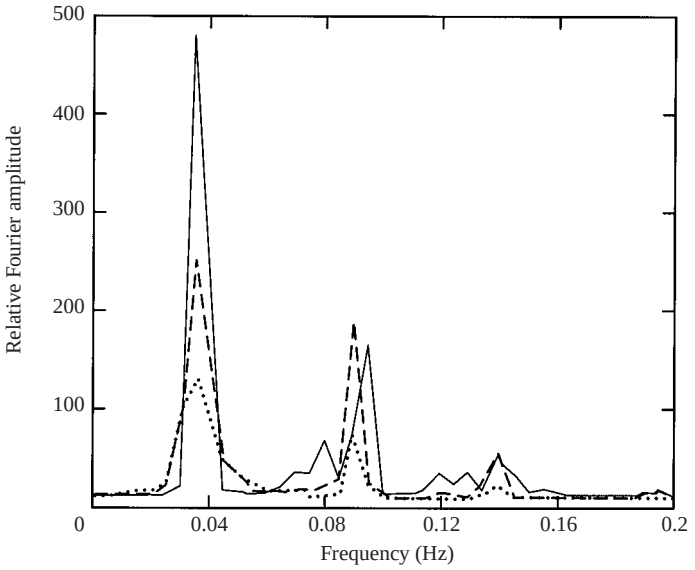

FIGURE 4. Fourier spectra for the same conditions $H = 4$ mm, $\Delta T = 2$ K and $\alpha = 0$ but from different radial positions. —, $r = 24$ mm; ----, $r = 30$ mm; · · · · ·, $r = 34$ mm. The peak amplitudes decrease from inside to outside in the proportion 480 : 240 : 115.

(Part 2, figure 17*d*). In an earlier microgravity experiment with a rectangular gap with $Ar = 1$ ($H = L = 2$ cm) time-dependent streaklines and a non-harmonic spectrum of temperature oscillations (Metzger *et al.* 1994) were observed, very much like the oscillation spectrum observed here in the annular gap. This and our observations indicate that the instability in the smaller Ar range is different from hydrothermal waves.

The thermocouples were placed to allow the extraction of the wavelength λ and phase velocity v, in the case of wavelike disturbances, by a correlation analysis of their signals. A wave crest would be detected earlier in time by the thermocouple at ($r = 24$ mm, $\alpha = 0°$) than by that at ($r = 30$ mm, $\alpha = 0°$) if the wave travels (partially) radially outwards. A prerequisite of the correlation analysis is well-defined temperature oscillations for all five thermocouples. The Fourier spectra must show the same peak to ensure a wave like disturbance. This was the case in the majority of steps near ΔT^c but not for the steps with ΔT much larger than ΔT^c. Even so, the signals can be interpreted as being caused by a travelling or a standing wave. The correlation analysis of the signals from different thermocouples showed that the flow state of travelling waves is a rare exception in the investigated parameter range. A correlation analysis of the data from the steps with $H = 2.5$ mm and with $H = 3.0$ mm, $\Delta T = 4$ K (figures 2*a* and 3) was possible in terms of the quality of the signals at all five thermocouples, and the Fourier spectra were the same at all five locations. With the unequal spacing of the thermocouple positions an unequivocal check for travelling waves is possible. But the correlation analysis of most steps did not fit what would be expected for travelling waves. A further confirmation for the absence travelling waves in some steps comes from the fact that the oscillation spectra from different locations are qualitatively different or quantitatively very different. Figure 5 shows such a temperature–time trace for $H = 6.0$ mm and $\Delta T = 5$ K with oscillations typical of the larger H and larger ΔT. These experimental findings show that the wavy

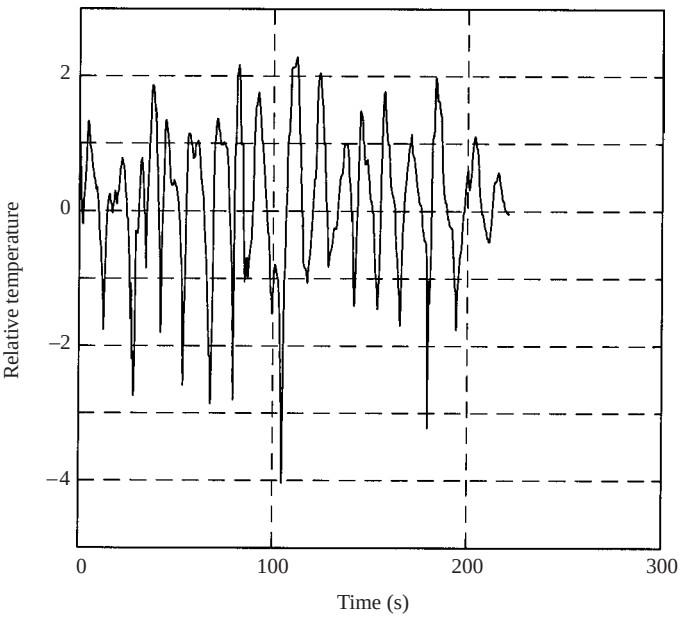

FIGURE 5. Temperature–time signal (smoothed) for $H = 6.0\,\mathrm{mm}$ and $\Delta T = 5\,\mathrm{K}$ from the thermocouple placed at $r = 24\,\mathrm{mm}$, $\alpha = 0$.

disturbances are either travelling waves or standing waves or waves travelling from a source in opposite directions and interfering in the opposite region of the annular gap, as observed by Schwabe (1999) in the larger Ar range. The reason for the waves appearing often as standing or counterpropagating ones could be residual gravity, e.g. with a component in the radial direction. But the same irregularities have sometimes been observed in experiments under normal gravity, which have been levelled precisely, showing that the system is prone to such 'defects'. Nevertheless we can report three cases with travelling waves; a case for H=6.0 mm with ΔT=2 K with a wave travelling only radially but not azimuthally (a standing wave like in Part 2 figures 12 and 13). In another case with $Ar = 5$ the correlation analysis of the thermocouple signals from different azimuthal positions indicates an azimuthally travelling pattern with mode $m = 8$ (eight wavetrains in the azimuthal direction) and a rotational speed of $0.2^\circ\,\mathrm{s}^{-1}$. For $Ar = 1$ we found an azimuthally travelling pattern with m between 5 and 6 and an angular speed of $(0.75 - 0.84)^\circ\,\mathrm{s}^{-1}$. The mode m found in the latter case is roughly comparable with the temperature pattern at the free surface visualized by the IR-camera (figure 12*a*).

3.2. *Observed critical and supercritical frequencies*

We now examine the problem of identifying the oscillatory state. Did we observe hydrothermal waves under microgravity? This question might be answered by comparing the frequencies and the wavelengths of the observed structures with the predictions. Figure 6 shows the periods τ of the oscillations at approximately $2Ma^c$ for various H. The period shows a strong increase with increasing H, close to that expected for hydrothermal waves in infinitely extended layers for $H \leqslant 10\,\mathrm{mm}$ (Schwabe *et al.* 1992; Riley & Neitzel 1998) and less strong for the higher H. The observed period is always greater than that expected for surface waves (Smith &

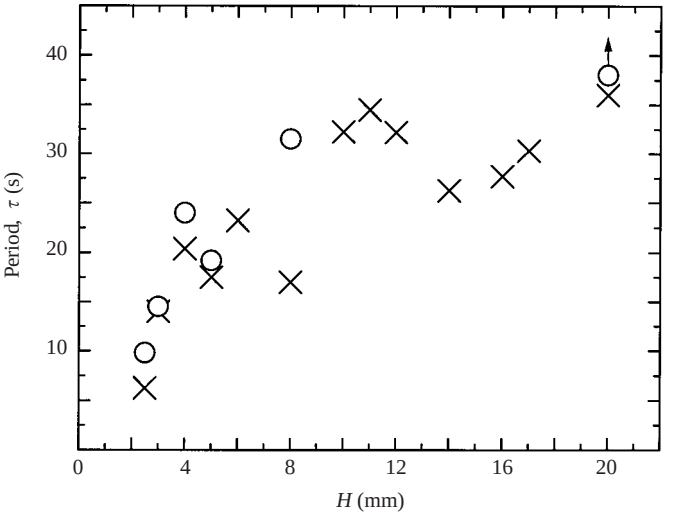

FIGURE 6. The period τ of the temperature oscillations near $2\Delta T^c$ to $3\Delta T^c$ for various H. The measurement points shown with circles are taken near $1.5\Delta T^c$, the points shown with crosses are taken near but below $3\Delta T^c$. The values of the τ in the low-H range are near those of hydrothermal waves in infinitely extended layers.

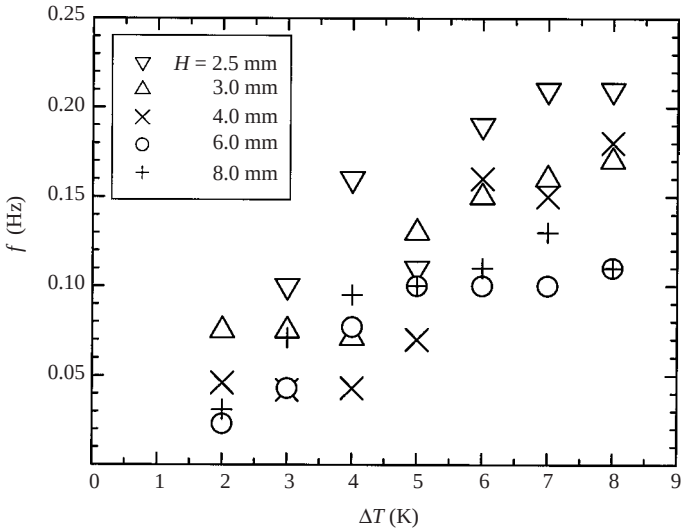

FIGURE 7. Dependence of the oscillation frequency f on ΔT for various H as recorded with the thermocouples.

Davis 1983). The scatter in the data is considerable and an agreement with the properties of hydrothermal waves is indicated but not very strongly.

The uncertainties in the period τ in figure 6 have various causes (in order of importance):

(i) We plot here τ near the threshold ($\Delta T = 3\,\mathrm{K}$ to $4\,\mathrm{K}$) but we do not have measurements for all H at exactly the threshold. Yet the frequency f can depend very strongly on ΔT as shown in figure 7.

(ii) The Fourier spectra showed more than one frequency peak or broadened peaks.

(iii) The Fourier spectra of the five thermocouples sometimes differ though they are taken at the same time.

The measurement points marked by circles in figure 7 are taken at $\Delta T = 2\,\mathrm{K}$ to 3 K, close to the threshold and display a significantly increased period. Figure 6 is a further hint that the instability is of hydrothermal-wave type for $H \leqslant 5\,\mathrm{mm}$ and probably of another type for $H \geqslant 8\,\mathrm{mm}$. We arrived at a similar conclusion in the discussion of the quality of the Fourier spectra and the basic flow structure in the preceding section.

Assuming a linear dependence of f on ΔT, the frequency f^c at the threshold $\Delta T^c \sim 1.5\,\mathrm{K}$ can be extrapolated in figure 7 for the five smallest values of H; f^c decreases with H as expected.

The increase of f with ΔT is roughly the same for all H in the displayed range up to $5\Delta T^c$ (figure 7). The constant c in $f = a + c\Delta T$ is the same for all H. On the other hand $f = F\gamma\mu^{-1}H^{-1}\Delta T$ with the non-dimensional frequency F defined in Part 2. According to figure 6 in Part 2, F is quite independent of ΔT for $H = 20\,\mathrm{mm}$ in the supercritical range up to $8Re_c$. Therefore from figure 7, $F(H)/H \sim$ constant. This is indeed the case for $Bi = 0$ (Part 2, figure 19*b*).

But the measured critical periods are considerably below the numerical ones (Part 2, figure 19*b*) with a constant negative offset for all H. Is this offset due to $Bi \neq 0$? It will be shown in § 3.5.2 that there was surface heating in our experiment, giving rise to $Bi \neq 0$. When this value of $Bi \neq 0$ is taken into account in the numerical simulation (Part 2, figure 20) good agreement for τ and for Ma^c is obtained.

3.3. *Measurement of the critical temperature difference for the onset of oscillations*

For all H realized we have some measurements of the temperature oscillation amplitude A in the supercritical ΔT range not too far above the threshold, and for some H we realized flow states $\Delta T < \Delta T^c$ with $A = 0$. Assuming a classical Hopf bifurcation, ΔT^c can be found by a linear extrapolation of $A^2(\Delta T)$ towards zero. From the examples in figure 8 one can expect a critical temperature difference ΔT^c around 2 K under microgravity in the investigated Ar range (figure 9). Besides this, we see an increase in ΔT^c towards $H = 2.5\,\mathrm{mm}$ and a minimum in ΔT^c around $H = 4\,\mathrm{mm}$ to 6 mm, corresponding to $Ar = 5$ to 3.3. This minimum is also found in the numerical results (Part 2, figure 19*a*) as a break in the curve $\mathrm{Re}_c(Ar)$. Because $Re_c \sim H$, the minimum in $Re_c(Ar)$ is not as obvious as the one in the plot of $\Delta T^c(H)$.

The ΔT^c values of figure 9 partly contradict the two independent two-dimensional numerical analyses for a fluid of almost identical Prandtl number by Peltier & Biringen (1993) and Xu & Zebib (1998); there the flow is found to be always stable for $Ar < 2.3$ and a double value for the transition steady $\leftrightarrow$ oscillatory is indicated e.g. for $Ar = 2.5$. This does not describe the three-dimensional reality as shown in figure 9; the flow becomes oscillatory in the stability region of two-dimensionl simulations. Since R_o does not exceed R_i by very much in our cylindrical geometry the results of the two-dimensional case should be approximately applicable. Further evidence against the two-dimensional numerical result comes from a sounding rocket experiment on thermocapillary convection in a rectangular gap with aspect ratio $Ar = 1$ (Metzger *et al.* 1994). These authors found rather chaotic temperature oscillations at comparable ΔT and Re in their experiment. Oscillations in cylindrical containers with $Ar < 1$ were also found under microgravity by Kamotani *et al.* (2000). This discrepancy between

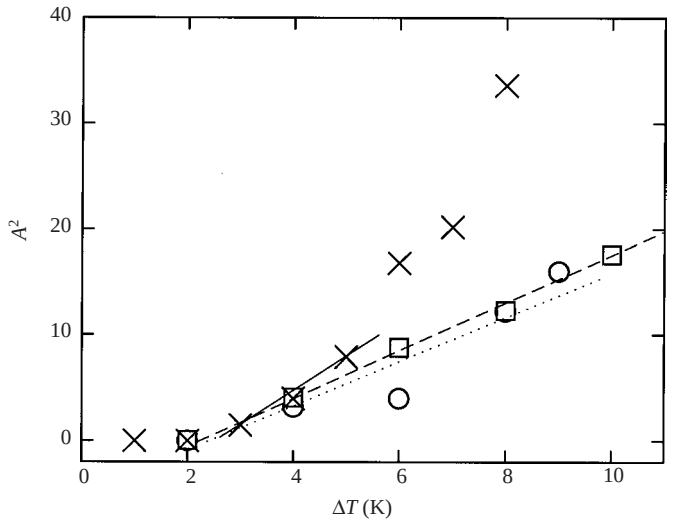

FIGURE 8. The squared amplitude A^2 of the temperature oscillations as function of the applied temperature difference ΔT: ×, —, $Ar = 8$; ○, ···, $Ar = 1.66$; □, – – –, $Ar = 1$. For $\Delta T = 1$ K and $\Delta T = 2$ K the uncertainty in A^2 is smaller than the symbol used and increases linearly with increasing ΔT to ± 7 for $\Delta T = 8$ K. The critical exponent is $a \leqslant 1$.

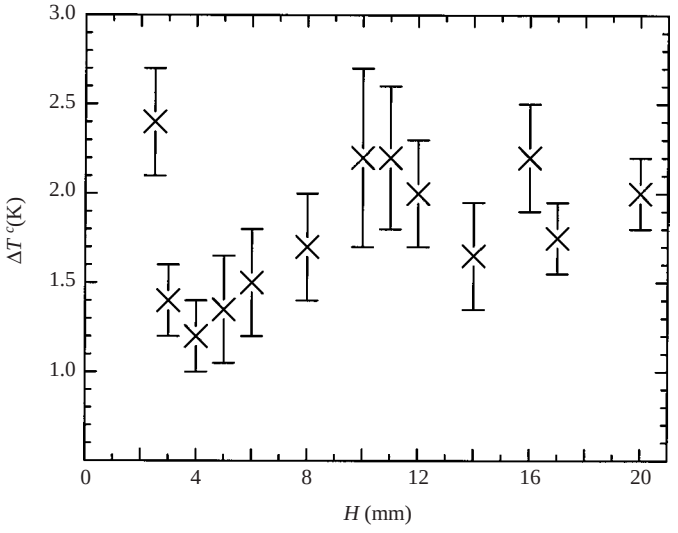

FIGURE 9. Critical temperature difference ΔT^c for the onset of temperature oscillations for various liquid heights H.

two-dimensional simulation and the experiments shows the need for three-dimensional numerical simulations of this system, which are performed in Part 2.

The deviation of the three-dimensional numerical results in Part 2 from the experimental ones is almost the same for $Ar = 8$ as that of the two-dimensional results but significantly larger for $Ar = 1$ (Part 2, figure 19*a*). As shown in § 3.5.2 of this paper and in Part 2 this discrepancy disappears when some heating of the surface, as occurred in the experiment, is taken into account.

We now compare our experimental microgravity results with those from Kamotani *et al.* (2000). These authors used much smaller containers with $Ar < 1$ in all cases, $R_i/R_o = 0.1$, $Pr = 27$, and heating of the inner cylinder. The heat source was more point-like than wall-like as in our case. For the $R_o = 6$ mm container their Ma_c was roughly twice ours and 2.5 times as high for the $R_o = 15$ mm container. Extrapolating the data of figure 13 of Kamotani *et al.* (2000) to $R_o = 80$ mm, one can predict for MAGIA a critical Marangoni number which is three times larger than actually measured by us. Taking into account that the onset of oscillations was estimated by Kamotani *et al.* (2000) from observations of the IR pattern at the free surface by eye, their value must be too high because it could not be extrapolated to zero since the 'signal-values' are only qualitative. But the Ma_c from Kamotani *et al.* (2000) supports the order of magnitude of ours, at least in the $Ar = 1$ range.

Ground-based experiments on shallow layers (Schwabe *et al.* 1992; Villers & Platten 1992) report an increasing ΔT^c for hydrothermal waves (or oscillatory states) with increasing H. The same is true for the travelling waves reported by Daviaud & Vince (1993). Unlike to these observations at normal gravity, we find a minimum in ΔT^c around H = 4 mm to 6 mm (which is near the maximum H investigated on the ground) and we do not find the increase in $\Delta T^c(H)$ predicted by Villers & Platten (1992). Thus we conclude that there must be a strong buoyancy influence on ΔT^c under normal gravity with H exceeding 2 mm.

3.4. *Flow structures detected by the IR-camera observing the temperature distribution at the free surface*

Due to limitations of the data storage capacity only 5 s of each measurement step (H, ΔT) were observed by the IR-camera. Because of the significantly larger period τ of the movements at the free surface no full period was observed. But the partial motion and the dynamics of the free-surface temperature distribution at higher supercritical Re are visible during these 5 s.†

The temperature patterns at the free surface are most impressive for the larger ΔT; in these cases the temperature resolution of 0.1 K of the IR-camera was sufficient. The noise in the IR-pictures can be averaged out by integrating over 1 s to 5 s. This is feasible for the smaller Ar and ΔT because the frequencies of the oscillations are low enough. The temperature patterns at the free surface are displayed in false colours (without any further manipulation) in the following figures.

3.4.1. *Multicells observed with the IR-camera*

Figure 10 shows the IR-picture from the free surface for $H = 2.5$ mm and $\Delta T = 6$ K. The window heater is glued slightly eccentrically to the ZnS window with the leads coming from about 9 o'clock. The central blue part is the top of the cooled inner cylinder with 40 mm ∅, partly visible under the dark red window heater which has a smaller diameter. Three concentric rings of almost homogeneous temperature fill the 20 mm gap (figure 10). The interface between the inner and the middle ring is not as sharp and circular because for $\Delta T = 6$ K the system is already oscillatory and the hydrothermal waves are strongest near the cold wall. All 75 IR-images of this step have been averaged in figure 10. The three concentric rings of approximately the same thickness are due to the multicellular structure already observed in shallow layers at normal gravity by Villers & Platten (1992), Schwabe *et al.* (1992), De Saedeler

† Two example video clips can be downloaded from the web: http://meyweb.physik.uni-giessen.de/meyer/crystalgrowth/video/homepage.html.

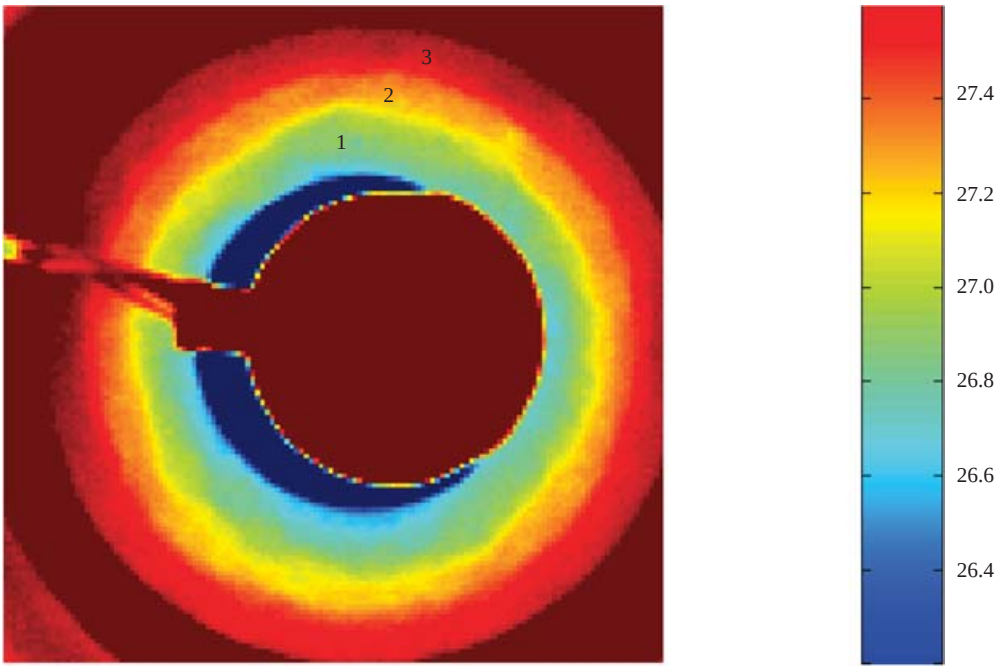

FIGURE 10. Averaged infrared pictures of the temperature distribution at the free surface for $H = 2.5$ mm and $\Delta T = 6$ K. Three concentric multicells fill the gap.

et al. (1996), Favre *et al.* (1997) and Riley & Neitzel (1998) who report stationary multicells. Under microgravity we find that multicellular flows are oscillatory. The multicell structure (MCS) and the hydrothermal waves can coexist up to at least $4Re_c$. Our observation of three cells for $H = 2.5$ mm and 2 cells for $H = 3.0$ mm indicates the relation $\lambda \approx 3H$ for the wavelength λ of the MCS. This is in good agreement with the observation of the multicells in shallow layers at normal gravity and with the numerical results in Part 2, figure 18(c, d).

Both, the MCS and the wavy states seem to occur at nearly the same Re_c under microgravity. This result differs from that of Earth-based experiments with the same silicone oil by Favre *et al.* (1997) who report a separation of these states by 1 K to 2 K. We have enough data to exclude this separation under microgravity.

We add that we could not observe longitudinal stationary rolls (axis parallel to the temperature gradient) as reported by Daviaud & Vince (1993) and later analysed by Mercier & Normand (1996). Mercier & Normand show that the longitudinal rolls appear under a dominating buoyancy effect which was not the case in our microgravity experiment. When we operated MAGIA under normal gravity with otherwise unchanged conditions we could clearly observe the longitudinal rolls as a 'spokes pattern' for $H \geqslant 6$ mm and the longitudinal rolls appeared down to $H = 2$ mm in a recent experiment with rectangular configuration in normal gravity (Benz & Schwabe 2001).

3.4.2. *Temperature pattern at the free surface*

The best examples of observed temperature patterns at the free surface are presented in figures 11 and 12 and compared with results from Part 2. Many of the other IR-pictures are spoiled by temperature asymmetries due to residual gravity as discussed below. Figures 11(a) and 11(b) show the temperature distributions for $H = 20$ mm at

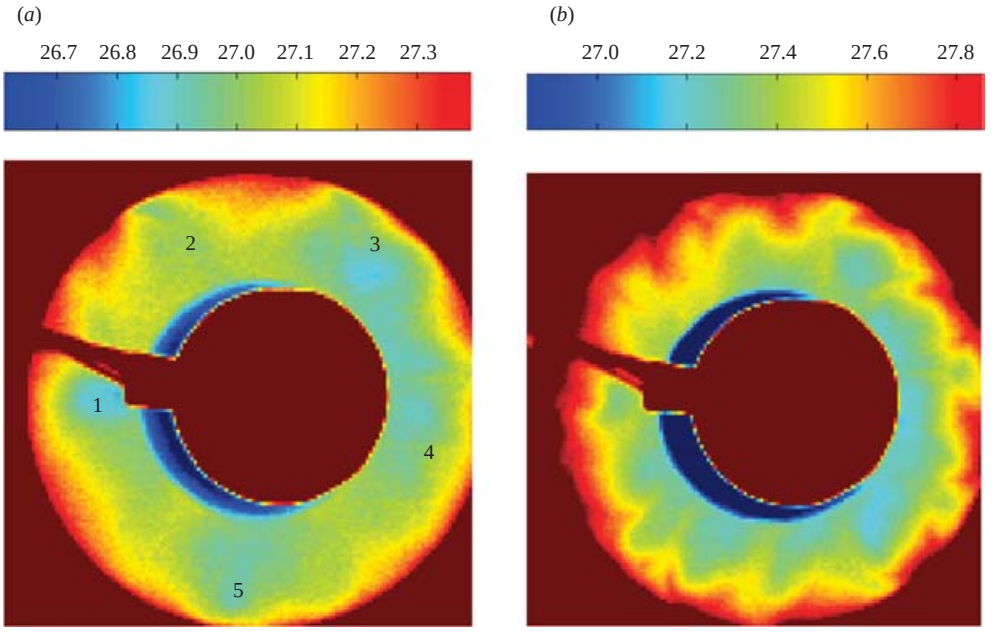

FIGURE 11. Averaged infrared pictures of the temperature distribution at the free surface for $H = 20$ mm showing fivefold symmetry $m = 5$ for the smaller ΔT. (*a*) $\Delta T = 4$ K, (*b*) $\Delta T = 8$ K.

$\Delta T = 4$ K and $\Delta T = 8$ K. $\Delta T = 4$ K corresponds approximately to $2Re_c$ and a fivefold temperature pattern is visible as in figure 4 of Part 2. The experimental pattern is more irregular than the corresponding numerical one at this *Re*. The irregularities in the fivefold pattern are definitely not due to an insufficient resolution of the IR-camera and are much stronger than in experiments at normal gravity (the same is true for the thermocouple signals). The frequency spectrum of these irregularities is higher than that of any time-dependent gravity disturbances during the flight. We therefore conclude that the irregularities are due to a slight symmetry breaking by residual gravity.

Figure 11(*b*) shows the surface temperature pattern for $H = 20$ mm at a high supercritical *Re* at $\Delta T = 8$ K.† The pattern is much more irregular than the corresponding numerical ones, figure 4 in Part 2. It resembles more the standing waves simulated for $Ar = 3.33$ at $Re = 900$ in figure 8(*b*) in Part 2. We know from experimental experience with thin layers in annular gaps under normal gravity that a small symmetry-breaking disturbance can produce counter-rotating (standing) waves from a travelling pattern, and that this disturbed pattern can persist even after the removal of the disturbance.

The number of waves *m* increases with decreasing *H* as shown in figure 12. Figure 12(*a*) shows $m = 5$ to 6 for $H = 17$ mm ($Ar = 1.17$) and $\Delta T = 4$ K. Figure 12(*b*) shows $m \approx 8$ for $H = 10$ mm ($Ar = 2.0$) and $\Delta T = 6$ K, and figure 12(*c*) shows $m \approx 11$ for $H = 8$ mm ($Ar = 2.5$) and $\Delta T = 5$ K. This is in good agreement with the numerical results in Part 2, figures 4, 7, 8, 11. The experimental pattern is again faint as discussed above but it is clearly visible that no pure wavetrains of a mode *m* have developed. Instead disturbed wavetrains or standing waves are found. In Part 2, figure 8, it can

† The dynamics at higher ΔT can be seen at http://meyweb.physik.uni-giessen.de/meyer/crystalgrowth/video/homepage.html in the files *MAGIA Microgravity result*.

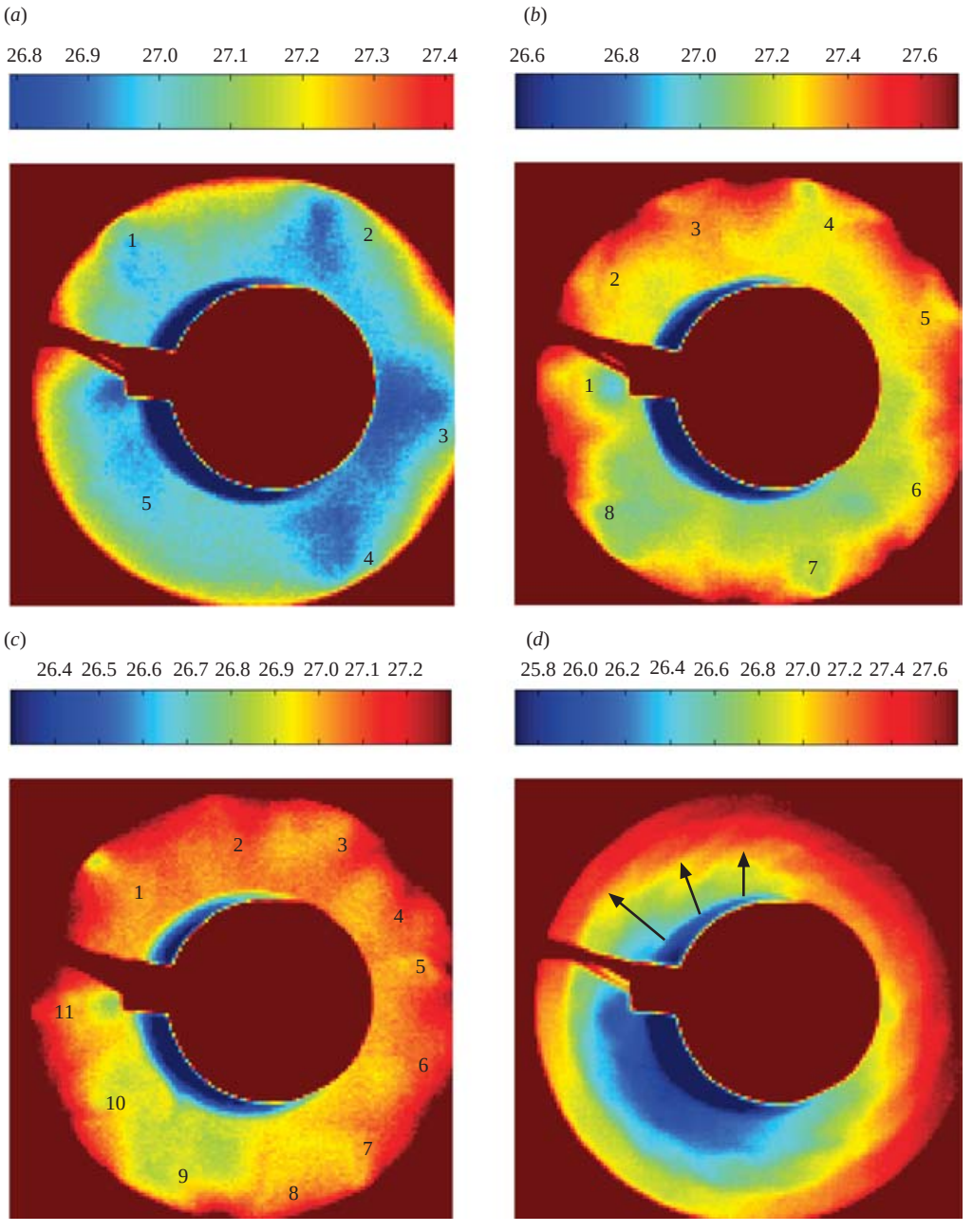

FIGURE 12. Averaged infrared pictures of the temperature distribution at the free surface for various H showing the increase of m with decreasing H. (*a*) $H = 17\,\text{mm}$, $\Delta T = 4\,\text{K}$, $m \approx 5{-}6$; (*b*) $H = 10\,\text{mm}$, $\Delta T = 6\,\text{K}$, $m \approx 8$; (*c*) $H = 8\,\text{mm}$, $\Delta T = 5\,\text{K}$, $m \approx 10{-}11$; (*d*) $H = 2.5\,\text{mm}$, $\Delta T = 5\,\text{K}$, spiral structures between 10 o'clock and 13 o'clock.

be seen that for $Ar = 3.33$ waves travelling from a 'source' in opposite directions can have already replaced rotating patterns at $Re = 900$. Consequently we cannot expect to observe experimentally ordered rotating wavetrains in the gap with $Ar = 2.5$ at $\Delta T = 5\,\text{K}$.

The fivefold surface temperature distribution (mode $m=5$) observed under microgravity in our large $Ar=1$ annulus compares well with earlier ground-based observations by Kamotani *et al.* (1992) and Kamotani & Masud (1996) who reported $m=2$ and $m=3$ rotating (and sometimes pulsating) patterns in small annuli heated from the inner wall with $Ar<1$. Later, Kamotani *et al.* (2000) reported on rotating and pulsating $m=2$ modes and rotating $m=3$ modes from a microgravity experiment with similar small annuli.

Figure 12(*d*) with $Ar=8$ and $\Delta T=5\,\mathrm{K}$ has three noticeable features. First, the multi-roll structure is again indicated. Second, we can observe one of the strongest hot–cold asymmetries found, pointing from about 2 o'clock towards 7 o'clock in this case. A dark cold plume extends towards 7 o'clock, most probably because of a residual gravity vector pointing in this direction. A main feature observed only for very few steps is the 'feathery' temperature structure in the middle of the annular gap. This is observed in the sector between 10 o'clock and 12 o'clock in figure 12(*d*). This is an indication of 'spiral arms' (hydrothermal waves in an annulus) already observed by Schwabe (1999) and Garnier & Chiffaudel (2001). It is clear that in the case of hydrothermal waves a spiral-like wave pattern (Archimedian spiral) will develop in annular geometry; for our liquid with $Pr=7$ the waves start at the cold inner cylinder with an angle $\beta\approx 60^\circ$ between the wave vector $\mathbf{k}$ and ∇T and travel towards the outer hot wall. ∇T is parallel to the radius vector. Because β is constant going outwards the wavefront will cross different radius vectors. Thus the wavefront must become a spiral. This is best seen in figure 11 of Garnier & Chiffaudel (2001) because they use an annulus with a large R_o/R_i. In Schwabe (1999) the spiral pattern looks different because of a reversed temperature gradient. In figure 16(*b*) from Part 2 one can count 20 spiral arms and the experimental estimate from the area with four faint spiral arms in figure 12(*d*) gives (18 ± 1) spiral arms for the full azimuth. The wavelength $\lambda\approx 2.5H$ predicted by Smith & Davis (1983) and by Riley & Neitzel (1998) yields 20 to 21 spiral arms in the gap with $Ar=8$ in the 'source-region' near the cold wall. It is interesting that in the numerical results in Part 2 the spiral arm separation is somewhat scattered and the spiral arm waves can travel counterclockwise in certain regions. According to the simulations one cannot expect to observe ordered spiral arms at $2Re_c$. Moreover, the wavetrains change either the number of waves or the wavelength on their way to the outer region. In figure 11 of Garnier & Chiffaudel (2001) it is seen that the spacing between the spiral arms increases towards the periphery.

Our simple assumption $\lambda\approx 2.5H$ for extended layers, near the cold wall, does not hold for smaller Ar in annular geometry; for $Ar=1$ it predicts $m=2$ to 3 whereas we observe experimentally and numerically 4 to 5 waves.

3.5. *Deviations from the ideal experiment*

3.5.1. *Residual varying gravity disturbances detected by the IR-camera*

The IR-pictures shown are exceptions because they display an almost rotationally symmetric temperature distribution in the gap (except for the dynamic structure due to thermocapillary flow). Most IR-pictures from different Ar–ΔT conditions show a hot–cold asymmetry in the gap as shown in figure 12(*d*). The dark area pointing towards 7 o'clock in figure 12(*d*) is colder than the opposite side. We assume that a significant component of the residual gravity points in this direction, which is most likely from an analysis of the gravity disturbances (Shevtsova *et al.* 2002). Thus we have a cold plume moving radially away from the cold cylinder against the thermocapillary flow. This temperature asymmetry has never been observed in the

normal gravity reference experiments with the same apparatus. Under normal gravity conditions the experiment is oriented with its cylinder axis exactly parallel to the gravity vector g_0. The asymmetry observed under microgravity changes its direction from time to time (Schwabe & Benz 2002), most probably due to the rotation of the satellite. Obviously, there were only a few situations during our IR-observations under microgravity with favourably low residual gravitation.

3.5.2. *Non-adiabatic free surface, $Bi \neq 0$*

It is not possible to realize exactly an adiabatic free surface ($Bi = 0$) in our experiment and similar ones. Let us consider radiative heat transport, heat by conduction and convection through the surrounding gas, and heat loss from the free surface by evaporation of the liquid. We define the mean temperature T_m of the liquid as $T_m = (T_o + T_i)/2 = 25\,^{\circ}\mathrm{C}$. T_o is the temperature of the sidewall of the annular gap, T_i the temperature of the cold central cylinder surface, and the temperature of the ZnS window is $T_w = 30\,^{\circ}\mathrm{C}$. The 2 cm wide gap between the liquid free surface and the inner side of the ZnS window was filled with air at normal pressure. Radiative heat transport between the various inner surfaces mentioned can be neglected in our case.

Conduction and convection in the gas gap pose a bigger problem in our case because $\delta T = T_w - T_m = 5\,\mathrm{K}$. Convection in the gas gap is not negligible even under microgravity because the streaming of the free surface will induce a parallel streaming in the air. Thus in the air gap of MAGIA air will be transported along the liquid surface towards the middle region, rise there, flow outwards along the ZnS window and warm up, flow down the sidewall of the gap and then again flow along the free surface. An analysis of the experimental conditions shows that in our case the free surface of the oil is heated from the outside by this mechanism because $\delta T \neq 0$. Let us remark that significant heat exchange by this mechanism cannot be avoided for liquids with $Pr > 1$ unless one works in vacuum. This is due to the fact that in our case the liquid surface temperature T_s is inhomogeneous for Re_c and, for most parts of the surface $(T_o + T_i)/2 < T_s \leqslant T_o$.

From ground-based experiments on evaporation and condensation of the same silicone oil under comparable conditions we can estimate the cooling of the free surface due to evaporation (Hintz 1999; Hintz, Schwabe & Wilke 2000). The evaporative cooling heat flux is $q_{evap} \approx 4\,\mathrm{W\,m^{-2}}$ near the oscillation threshold. The conductive–convective heating of the free surface by the hotter ZnS window is $q_{advect} \approx 10\,\mathrm{W\,m^{-2}}$. This was derived from an estimate of $Nu \approx 2$ for the convective heat transport in the gas gap near ΔT^c. Thus the free surface is effectively heated by $6\,\mathrm{W\,m^{-2}}$. From the IR-camera measurement we know that the oil free surface has a temperature of approximately 26 °C near ΔT^c, which gives $\delta T = T_w - T_{oilsurface} \approx 4\,\mathrm{K}$. Accordingly the heat transfer coefficient is $h = 1.5\,\mathrm{W\,m^{-2}\,K^{-1}}$ and the Biot number is $Bi = 0.3$ for the heat input to the free surface.

The use of $Bi = 0.3$ in the simulations gave good agreement with the experimental Re_c and τ_c (figure 20 in Part 2). Calculations with unrealistic and not justified high cooling ($Bi = 20$) only bring the numerical Re_c and τ_c nearer to the measured values.

4. Summary and conclusions

Thermocapillary flow in open cylindrical annuli of various aspect ratios has been investigated experimentally under microgravity. We report the critical temperature differences ΔT^c for the onset of oscillatory flow with a minimum around aspect

ratio $Ar = 4$. The experimental values of ΔT^c are larger and the experimental oscillation periods near the threshold are smaller than the corresponding numerical ones calculated for an adiabatic free surface. An analysis of the heat balance of the free surface revealed heating of the surface by the hotter ZnS window above the annular gap, and the numerical results for Re_c and τ_c taking this into account are close to the experimental ones.

Based on the measurements of the critical oscillation frequencies f^c and temperature pattern by an IR camera at the free surface, the oscillatory flow states in the higher Ar range could tentatively be interpreted as hydrothermal waves (Smith & Davis 1983). But the signals correspond more to standing waves than to travelling waves. Furthermore, coincidence of multicells (multirolls) with the hydrothermal waves was found in the large Ar range. In the range of small Ar we found m-fold temperature patterns in the gap, e.g. $m = 5$ for $Ar = 1$, m decreasing with decreasing Ar.

In the supercritical range above $4Re_c$ the IR temperature patterns and the Fourier spectra from thermocouple measurements become more complex. The frequency f as function of ΔT could be measured only in the range of higher Ar.

Both experimental and numerical results are very sensitive to heat input at the free surface. The heat fluxes through the free surface need to be measured in future experiments for accurate analysis. In crystal growth from the melt under microgravity, and most probably under normal gravity as well, the critical Reynolds number can be effectively increased and temperature oscillations with growth rate fluctuations and growth striations can be effectively suppressed by additional heating of the melt free surface.

This paper is dedicated to Professor Dr A. Scharmann on the occasion of his 75th birthday.

The experiment and the flight were financed by the European Space Agency ESA. The ground-based activities of Dietrich Schwabe were supported by the BMBF through DLR under contract No. 50 WM 9446. He thanks these institutions for their invaluable financial support. We thank Simon Benz for his valuable help in preparing this experiment, the Russian colleagues and many other helpers for the professional satellite flight and the operation of the telesupport facility. The project would not have been possible without the personal commitment of the engineers from Verhaert D & D (Belgium), the engineers from ESA (especially Antonio Verga) and many others.

REFERENCES

Benz, S. & Schwabe, D. 2001 The three-dimensional stationary instability in dynamic thermocapillary shallow cavities. *Exps. Fluids* **31**, 409–416.

Busse, F. H., Pfister, G. & Schwabe, D. 1998 Formation of dynamical structures in axisymmetric fluid systems. In *Evolution of Spontaneous Structures in Dissipative Continuous Systems*. Lecture Notes in Physics vol. 55 (ed. F. H. Busse & S. C. Mueller), pp. 86–126. Springer.

Daviaud, F. & Vince, J. M. 1993 Travelling waves in a fluid layer subjected to a horizontal temperature gradient. *Phys. Rev.* E **48**, 4432–4436.

De Saedeler, C., Garcimartin, A., Chavepeyer, G., Platten, J. K. & Lebon, G. 1996 The instability of a liquid layer heated from the side when the upper surface is open to air. *Phys. Fluids* **8**, 670–676.

Favre, E., Blumenfeld, L. & Daviaud, F. 1997 Instabilites of a liquid layer locally heated on its surface. *Phys. Fluids* **9**, 1473–1475.

Garnier, N. & Chiffaudel, A. 2001 Two-dimensional hydrothermal waves in an extended cylindrical vessel. *Eur. Phys. J.* B **19**, 87–95.

Hintz, P. 1999 Konvektion im Czochralski-Tiegel. PhD thesis, University Giessen.

Hintz, P., Schwabe, D. & Wilke, H. 2000 Convection in a Czochralski crucible-Part 1: non-rotating cryst. *J. Cryst. Growth* **222**, 343–355.

Hurle, D. T. J. & Cockayne, B. 1994 Czochralski growth. In *Handbook of Crystal Growth, Part 2A Basic Techniques* (ed. D. T. J. Hurle), pp. 99–211. North-Holland.

Kamotani, Y., Lee, J. H. & Ostrach, S. 1992 An experimental study of oscillatory thermocapillary convection in cylindrical containers. *Phys. Fluids* A **4**, 955–962.

Kamotani, Y. & Masud, J. 1996 Oscillatory convection due to combined buoyancy and thermocapillarity. *J. Thermophys. Heat Transfer* **10**, 102–108.

Kamotani, Y., Ostrach, S. & Masud, J. 2000 Microgravity experiments on oscillatory thermocapillary flow in cylindrical containers. *J. Fluid Mech.* **410**, 211–233.

Kuhlmann, H. C. 1999 *Thermocapillary Convection in Models of Crystal Growth.* Springer.

Mercier, J. F. & Normand, C. 1996 Buoyant-thermocapillary instabilities of differentially heated liquid layers. *Phys. Fluids* **8**, 1433–1448.

Metzger, J., Schwabe, D., Cramer, A. & Scharmann, A. 1994 Marangoni convection in a rectangular open cavity in microgravity. In *Final Reports of Sounding Rocket Experiments in Fluid Science and Materials Science* – TEXUS 28-30, Maser 5 & MAXUS 1, ESA SP-1132 (Vol. 4), pp. 60–71.

Peltier, L. & Biringen, S. 1993 Time-dependent thermocapillary convection in a rectangular cavity: Numerical results for a moderate Prandtl number fluid. *J. Fluid Mech.* **257**, 339–357.

Riley, R. & Neitzel, G. 1998 Instability of thermocapillary-buoyancy convection in shallow layers. Part 1. Characterization of steady and oscillatory instabilities. *J. Fluid Mech.* **359**, 143–164.

Schwabe, D. 1984 Oscillatory thermocapillary convection in a horizontal shallow liquid layer heated from a sidewall. *5th Intl Conf. on Physico-Chemical Hydrodynamics, December 16–21, 1984, Tel-Aviv, Israel, Abstract Book*, pp. 127–128.

Schwabe, D. 1988 Surface-tension-driven flow in crystal growth melts. In *Crystals*, vol. 11 (ed. H. C. Freyhardt), pp. 75–112. Springer.

Schwabe, D. 1999 Microgravity experiments on thermocapillary flow phenomena: Examples and perspectives. *J. Japan Soc. Microgravity Appl.* **16**, 1–6.

Schwabe, D. & Benz, S. 2002 Thermocapillary flow instabilities in an annulus under microgravity – results of the experiment MAGIA. *Adv. Space Res.* **29**, 629–538.

Schwabe, D., Moeller, U., Schneider, J. & Scharmann, A. 1992 Instabilities of shallow dynamic thermocapillary liquid layers. *Phys. Fluids* **4**, 2368–2381.

Shevtsova, V. M., Melnikov, D. E. & Legros, J. C. 2002 The post-flight analysis of micro-acceleration on-board of the Russian Spacecraft FOTON-12. *ESA Contract Report*.

Sim, Bok-Cheol, Zebib, A. & Schwabe, D. 2003 Oscillatory thermocapillary convection in open cylindrical annuli. Part 2. Simulations. *J. Fluid Mech.* **491**, 259–274.

Smith, M. & Davis, S. 1983 Instabilities of dynamic thermocapillary liquid layers. Part 1. Convective instabilities. *J. Fluid Mech.* **132**, 119–144.

Villers, D. & Platten, J. K. 1992 Coupled buoyancy and Marangoni convection in acetone: experiments and comparison with numerical simulations. *J. Fluid Mech.* **234**, 487–510.

Xu, J. & Zebib, A. 1998 Oscillatory two- and three-dimensional thermocapillary convection. *J. Fluid Mech.* **364**, 187–209.